THE ASTROPHYSICAL JOURNAL, 498:851–862, 1998 May 10

SPECTRAL SYNTHESIS OF TiO LINES

JEFF A. VALENTI[1]
NOAO, P.O. Box 26732, Tucson, AZ 85726-6732; jvalenti@noao.edu
NIKOLAI PISKUNOV[1]
Astronomical Observatory of Uppsala University, Box 515, S-751 20 Uppsala, Sweden; piskunov@astro.uu.se
AND
CHRISTOPHER M. JOHNS-KRULL[2]
JILA, University of Colorado, Boulder, CO 80309-0440; cmj@sunburst.ssl.berkeley.edu
Received 1997 October 6; accepted 1997 December 23

ABSTRACT

We explore the extent to which current titanium oxide (TiO) line data and M dwarf model atmospheres can be used to reproduce an $R = 120{,}000$ optical spectrum of the relatively inactive star Gliese 725B (M3.5 V). We find that tabulated TiO wavelengths have errors large enough to complicate line identification, especially for transitions involving higher vibrational states. We determine empirical wavelength corrections for 12 strong γ-bands near 6680 and 7090 Å. For the sequence of orbital quantum numbers, J, within any one of these bands, our observations confirm the predicted line spacing, thereby validating the rotational constants for low vibrational levels. However, the predicted wavelengths have zero-point errors that differ for each overlapping band. Next, we compare observed and synthetic spectra near 8463 Å, where an ϵ Q_3 0–0 band head is expected, demonstrating that the electronic oscillator strength of 0.014 advocated by Jørgensen is too large by at least a factor of 5. This has a minor effect on the structure of theoretical model atmospheres. Using our empirically corrected TiO wavelengths, we compute a grid of synthetic spectra for Allard & Hauschildt models spanning a range in effective temperature ($T_{\rm eff}$), surface gravity (log g), and metallicity ([M/H]). Interpolating in this grid of synthetic spectra, we simultaneously fit observations of the TiO band head region near 7088 Å and five Ti I and Fe I lines near 8683 Å. For Gl 725B, we find $T_{\rm eff} = 3170 \pm 71$ K, log $g = 4.77 \pm 0.14$, [M/H] $= -0.92 \pm 0.07$, and $v_{\rm mac} = 1.1 \pm 0.7$ km s^{-1}. We show that by using both atomic and molecular lines as constraints, systematic uncertainties in derived stellar parameters can be reduced. These parameters are consistent with published values obtained by other means, but more stringent tests would be useful. In the Appendix, we tabulate wavelengths, identifications, relative line strengths, and other properties of the strongest band heads in the α, β, γ, γ', δ, ϵ, and ϕ electronic systems of TiO.

Subject headings: atomic data — molecular data — stars: fundamental parameters — stars: individual (Gliese 725B) — stars: low-mass, brown dwarfs

1. INTRODUCTION

Detailed knowledge about physical processes in stellar envelopes comes primarily from the interpretation of observed spectra. As computers and data quality have improved, coarser characterizations of stellar spectra (photometric colors, molecular band depths, line equivalent widths) have given way to direct synthesis of stellar spectra (e.g., Valenti & Piskunov 1996; Anstee, O'Mara, & Ross 1997) using ever improving model atmospheres. Spectrum synthesis is now used to study a wide variety of phenomena in stars, including peculiar abundances, magnetic fields, surface structure, differential rotation, and stellar winds. The goal is to synthesize spectra accurately enough to study these and other stellar phenomena. In this paper, we are particularly interested in assessing how well we can model TiO bands and atomic features in a high-resolution ($R = 120{,}000$) optical spectrum of the cool dwarf Gliese 725B (M3.5 V).

Meaningful spectrum synthesis depends on accurate atomic and molecular data, good model atmospheres, and a radiative transfer code that incorporates all the relevant physics. For the study of cool stars (or cool spots on warmer stars), the accuracy of molecular data is a particular concern, since molecules affect both the detailed structure of the spectrum (through the action of individual lines) and the global structure of the atmosphere (through the cumulative effects of all line and continuous opacity, for example). In particular, infrared water bands strongly influence the global structure of the atmosphere and hence the spectrum (Auman 1969; Mould 1976; Allard & Hauschildt 1995b; Allard et al. 1997). Red spectra of M stars are dominated by TiO bands, which have become the primary means of establishing spectral types (Kirkpatrick, Henry, & McCarthy 1991; Reid, Hawley, & Gizis 1995). Therefore, it is particularly important to know the quality of tabulated wavelengths and oscillator strengths for this molecule. Detailed spectroscopic studies are needed to study how TiO band depth depends on temperature, gravity, and chemical composition.

Given the diagnostic potential of spectrum synthesis, there have been remarkably few published attempts to model observed spectra of M dwarfs. Mould (1978) derived $T_{\rm eff}$ and [M/H] (metallicity) for a few early M dwarfs by comparing synthetic spectra based on his own model atmospheres (Mould 1976) with near-IR Fourier Transform Spectrometer (FTS) spectra (4000–6600 cm^{-1}, $R \sim 18{,}000$). Naftilan, Sandmann, & Pettersen (1992) used the same models and a radiative transfer code by Kurucz (1993a,

[1] Formerly at JILA, University of Colorado, Boulder, CO 80309-0440.
[2] Now at Space Sciences Laboratory, UC Berkeley, Berkeley, CA 94720.

1993b) to model blue spectra ($\lambda \sim 4000$ Å, $R \sim 30{,}000$) of AD Leo. Brett (1990) determined astrophysical oscillator strengths for TiO and VO bands by modeling red and IR spectra ($R \sim 500$) of M giants. All of these studies used approximate methods for treating the molecular line opacity.

Brett & Plez (1993) computed synthetic spectra for their grid of M dwarf models, comparing them with the low-resolution observations of Bessel (1991). Better opacity sampling techniques allowed a more realistic connection between the effective temperature scale of the grid and the empirical $T_{\rm eff}$ scale of Bessel. However, the resolution of the observed spectra was too low to take full advantage of the temperature sensitivity of individual molecular features.

More recently, Kirkpatrick et al. (1993) determined $T_{\rm eff}$ for a sequence of M dwarfs by comparing spectra computed by Allard (1990) with red ($R \sim 500$) and IR ($R \sim 250$) spectra of M dwarfs. The original model atmospheres of Allard are continually being improved (Allard & Hauschildt 1995a, 1998, hereafter AH95 and AH98). These updated atmospheres have been used to model spectra (1.16–1.22 μm, $R \sim 1100$) of a sequence of M dwarfs (Jones et al. 1996), an optical spectrum ($R = 60{,}000$) of the M8 Ve star VB10 (Schweitzer et al. 1996), and the IR spectrum (1–2.5 μm) of the brown dwarf Gl 229B (Allard et al. 1996). Our study presented here differs from the work just described in that we use a very high resolution ($R = 120{,}000$) optical spectrum of a moderately warm M dwarf to assess the quality of TiO line data and the model atmospheres. Similar resolution spectra occasionally *have* been used (with great success) in studies of other astrophysical sources, for example, sunspot umbrae (Lambert & Mallia 1972) and the red supergiant VY Canis Majoris (Phillips & Davis 1987).

In the next section, we describe certain key requirements for a detailed spectral synthesis of TiO, namely, the molecular equation of state, atomic and molecular opacities, and a grid of model atmospheres. In § 3 we compare synthetic spectra with a high-resolution, high signal-to-noise (S/N) observation of Gl 725B (M3.5 V). We find and correct significant errors in the best available wavelengths for TiO lines. We then demonstrate that the (supposedly quite strong) ϵ bands are much weaker than expected, implying a large error in the electronic oscillator strength. Finally, we determine $T_{\rm eff}$, log g, [M/H], and $v_{\rm mac}$ for Gl 725B using various atomic lines and TiO γ-bands as constraints. In § 4 we compare with predictions from the literature and comment on the current usefulness of spectrum synthesis as a tool to analyze K and M stars.

2. MOLECULAR LINE SYNTHESIS

Generating high-resolution, synthetic spectra of TiO lines in cool stars is procedurally very similar to synthesizing spectra of atomic lines in warmer stars, although many more lines are involved. The only algorithmic change occurs in the equation of state routine, which must be extended to include molecules (and dust formation in cool brown dwarfs). Synthetic spectra still depend, however, on molecular data and model atmospheres of unknown quality.

2.1. *Equation of State*

Cooler temperatures affect spectral line formation in several ways. Atoms combine to form molecules, replacing atomic line opacity with a richer spectrum of molecular line opacity. Conversely, continuous opacity generally decreases in the optical and infrared, as H_2 and H_2^+ replace H^- and H as the dominant sources of continuous opacity. Ionization of atomic and molecular species decreases, reducing the importance of line broadening due to electron and ion collisions. At low enough temperatures and densities, collisions are no longer frequent enough to maintain local thermodynamic equilibrium (LTE). In our analysis we assume LTE, which is a good assumption over most of the line formation region. Departures from LTE will be significant high in the atmosphere, so the cores of the strongest features in our synthetic spectra could potentially be affected (Hauschildt et al. 1997). In fact, we do not accurately reproduce the line cores (see § 3.4), but non-LTE effects are just one possible explanation for this discrepancy.

To calculate the equilibrium balance between ions, atoms, and molecules, we need ionization potentials, molecular dissociation energies (at 0 K), and chemical equilibrium constants as a function of temperature. Note that equilibrium constants can be computed directly from partition functions, but we have employed separate fits. In this study, we used atomic data from the ATLAS9 code (Kurucz 1993a, 1993b), which are valid in the temperature range 2000 K $< T <$ 100,000 K. For molecules, we initially followed Sauval & Tatum (1984) for diatomics and Irwin (1988) for polyatomics. Using these data, we were able to reproduce Allard & Hauschildt (AH) partial pressures for major species (H_2, H_2O, CO, and TiO) to better than 1% in a test case, but errors were large for certain minority species. For the sake of consistency with the atmospheric models, we ultimately decided to adopt the AH equilibrium constants, which we reconstructed by fitting fifth-order polynomials to partial pressure data for 196 molecular species as a function of log (5040/T). Our fits are valid in the temperature range 1600 K $< T <$ 7730 K, which encompasses all of the temperatures present in our grid of models. We use the molecular partition function from Sauval & Tatum (1984) for TiO.

The equilibrium state of matter for a given temperature and gas pressure is specified by the partial pressure (or, equivalently, the number density) of every chemical species. Charge conservation, total pressure, and abundance constraints are linear in the partial pressures; whereas chemical ionization and equilibrium constraints are linear in the logarithm of the partial pressures. To solve the combined, nonlinear system of equations, we have adapted a code by Bennett (1983). The full set of equations is linearized and then solved iteratively using a Newton-Raphson technique with quadratic convergence near the solution. An adequate starting approximation is obtained by apportioning gas pressure according to elemental abundances, allowing for ionization, and then analytically solving for the equilibrium state of a simplified chemical system consisting of H, He, C, O, Ne, H_2, CO, and H_2O. For computational economy, Bennett combined trace elements into a single fictitious element, but we solve the full problem, which is small by modern standards.

We compared our derived equilibrium state for certain test cases with other codes and published results. Bennett (1983) provides plots of partial pressure for the most important chemical species over a wide range of temperatures (1500 K $< T <$ 6000 K). We are able to reproduce the qualitative behavior of these plots with only minor quantitative

differences that can be attributed to differences in atomic and molecular data. We have also compared our partial pressures with detailed calculations provided by (P. Hauschildt 1997, private communication) for a realistic stellar atmosphere (AH95, AH98). There are some discrepancies as large as 10% for minority species, which we attribute to differences in our atomic partition functions. For significant species, however, agreement is better than 1% throughout the atmosphere.

2.2. *Continuum and Line Opacities*

Calculating the continuous opacity is relatively straightforward, once the number densities of important species (e.g., H, H^-, H_2, etc.) are known. We use the continuous opacity routines from ATLAS9 (Kurucz 1993a, 1993b) for all species except H^-, which we treat using an analysis (John 1988) of the best available wave functions. We compared our continuous opacities in the spectral interval 8465–8472 Å with those obtained by (F. Allard and P. Hauschildt 1997, private communication) for one of their $T_{\rm eff} = 3500$ K model atmospheres (AH95, AH98), again achieving agreement to better than 1% throughout the atmosphere.

Even for a small spectral interval, determining line opacity requires considerable effort. Operationally, the difficulty arises from the need to sift through millions of transitions, searching for lines in the wavelength interval of interest. As a relevant illustration, the TiO line list of Jørgensen (1994) contains 12 million lines. Except for the ϵ system (see § 3.3), we used the electronic oscillator strengths from Table 1 of Jørgensen (1994) to convert the tabulated line strength parameter to actual log gf values. Before synthesizing spectra for a large grid of model atmospheres, we trimmed insignificantly weak lines from the list to reduce the calculation time. All lines were ranked according to their strength, S, as defined in the Appendix with a temperature of 3000 K. Lines below a threshold, denoted by $S_{\rm thr}$, were neglected. For a characteristic model atmosphere, we progressively subtracted 0.5 from $S_{\rm thr}$ until the maximum change in residual intensity (at $R = 120{,}000$) was below 0.5% throughout the wavelength interval. Only lines stronger than this final threshold were used in subsequent analyses. We obtained $S_{\rm thr}$ of 0.25 and 0.38 for echelle orders 40 and 49 (see § 3), yielding 1644 and 9035 spectral lines, respectively.

In cooler stars, atomic lines become progressively weaker because thermal energy less effectively populates higher atomic states and because atoms are depleted by the formation of molecules and grains. Nonetheless, atomic lines are important diagnostics that complement the molecular lines. Gathering atomic line data would also be a chore were it not for the Vienna Atomic Line Database (VALD; Piskunov et al. 1995). This electronic service culls through an extensive database of atomic lines (including the compilations by Kurucz) to find the small subset of lines that are relevant in a particular spectrum synthesis application.

In the spectral synthesis described below, the only molecular lines we consider are those due to TiO. Many other molecular species contribute to the structure of the atmosphere (and were considered in the construction of the models), but in the synthesis discussed below, other molecules can be ignored (P. Hauschildt 1997, private communication). A service analogous to VALD, but for molecular lines, would be extremely valuable.

2.3. *Atmospheres for Cool Stars*

In general, determining stellar atmospheric structure and the corresponding radiation field are coupled problems. This is particularly true in cool stars, where molecular bands have a dramatic effect on the radiation field and hence on the thermal structure of the atmosphere. When computing atmospheric structure, however, it can be more efficient to approximate the wavelength dependence of the opacity, using distribution functions, sampling, or some related technique. In fact, for molecules with adequate data, AH treat line opacity directly with depth dependent Voigt (or Gaussian) absorption profiles for each line above some opacity threshold. Using this approach, modest errors in transition wavelengths should have little effect on the derived atmosphere. However, wavelength errors can (and do) distort detailed synthetic spectra. In this study, we adopt model atmospheres and then study the *detailed* behavior of the emergent spectrum.

All of our tests were carried out with "next generation" model atmospheres of AH, computed with version 7.4.1 of the PHOENIX code, dated 1997 January 5. These models were calculated using an elaborate equation of state and extensive molecular line lists. Moreover, the models are electronically accessible. Other grids of model atmospheres for M dwarfs have been presented by Mould (1976), Allard (1990), and Kui (1991). In this study, we focus primarily on the current state of the molecular line data, only peripherally commenting on possible errors in the model atmospheres.

3. APPLICATIONS

3.1. *Observations and Data Reduction*

On 1995 August 20, we obtained a spectrum of Gl 725B using the 2.7 m Harlan J. Smith telescope at McDonald Observatory to feed a cross-dispersed, echelle spectrograph (Tull et al. 1995). A slit width of 0.″59 resulted in a measured resolving power of 121,000. With a Tektronix 2048 × 2048 CCD at the F1 coudé focus, each resolution element mapped into 4.65 pixels. Gl 725B was observed for total of 1.9 hr, split into two exposures to facilitate cosmic-ray removal.

Spectra were reduced using an automated echelle reduction package (Valenti 1994) written in the Interactive Data Language (IDL). After image calibration, the residual fringing, scattered light, and wavelength-dependent flat-field variations were less than 1%. In the final one-dimensional spectrum, we achieved an S/N of 270 pixel^{-1}, consistent with Poisson statistics for the number of observed stellar photons. We determined a wavelength scale by fitting a two-dimensional polynomial to $m\lambda$ as function of pixel and order number m for a total of 97 thorium lines, yielding a maximum error of 0.005 Å.

Because of the high resolving power of the spectrograph, only a portion of each echelle order can be recorded in a single exposure. Using the E2 grating, we obtained about 27 Å per order in 19 orders ($m = 37$–55), spanning the wavelength range 6306–9407 Å. The data presented here were originally gathered to study magnetic fields in M dwarfs (Johns-Krull & Valenti 1996), so we miss some of the strongest TiO bands. We do, however, observe the $\gamma\, R_2$ 1–0, $\gamma\, R_2$ 0–0, $\epsilon\, R_3$ 2–1, and $\epsilon\, Q_3$ 0–0 band heads.

Despite prevalent molecular absorption in spectra of M stars, the curvature of the echelle blaze function can often be

removed empirically from an observation because the distribution of line depths is similar across the spectrum. However, when strong band heads distort the apparent shape of the blaze function, independent constraints are needed. For our echelle order 49, which contains the strong γ R_2 0–0 of TiO, we interpolated blaze functions determined empirically for nearby orders. With this one exception, blaze functions were determined locally and removed from each echelle order.

3.2. TiO *Wavelength Errors*

The strongest TiO features in our spectrum of Gl 725B occur in echelle order 49. The observed wavelength interval (7078–7103 Å) contains over 40,000 TiO lines, mainly from the γ system ($A\,^3\Phi - X\,^3\Delta$). About 9000 of these lines contribute significantly to the final spectrum. In order 49, the strongest lines connect ground vibrational states (0–0), whereas in order 52, the strongest lines arise from 1–0 vibrational transitions. Below, we use lines in orders 49 and 52 to test the TiO wavelengths tabulated by Jørgensen (1994).

Initially, we calculated a synthetic spectrum of Gl 725B using Jørgensen (1994) line data and a preliminary AH model with $T_{\rm eff} = 3500$ K, log $g = 5.0$, [M/H] = 0, and v sin $i = 0$ km s^{-1}. This allowed us to identify and correct wavelength errors in the TiO line list, but *all* figures in this paper use actual stellar parameters (see § 3.4). Figure 1 compares a synthetic spectrum with the observed spectrum of order 49 (broken into six panels for clarity). The synthetic spectrum has been convolved with a Gaussian to match the resolution of the observations. Since we do not have a flux-calibrated spectrum, normalization of the observed spectrum depends on the synthetic spectrum, as discussed in § 3.4. Although the observed and synthetic spectra have similar distributions of residual intensity, individual strong lines are displaced, and weak features are distorted. These discrepancies in the synthetic spectrum are primarily due to wavelength errors in the Jørgensen (1994) line list.

To illustrate, we use vertical line segments in Figure 1 to indicate the predicted wavelengths of the Q_2 (*dotted vertical lines*) and Q_3 (*dashed vertical lines*) branches. The number in parentheses above each designated spectral line is the rotational quantum number of the molecule in the ground electronic state. Notice that for each predicted line in the Q_3 branch, a corresponding feature in the observed spectrum is displaced *redward* by 0.05 Å. However, for the Q_2 branch, the observed features are displaced *blueward* by 0.04 Å. Because the two branches overlap in wavelength and span much of the echelle order, the discrepancies cannot both be due to errors in the observed wavelength scale. The only remaining explanation is that the Jørgensen (1994) line list has systematic errors in wavelength.

For several TiO branches, we visually estimated errors in the Jørgensen (1994) wavelengths to the nearest 0.005 Å. Tables 1 and 2 give the resulting corrections (in Å) that must be applied to the Jørgensen (1994) wavelengths to match our observed spectrum of Gl 725B. For ^{48}Ti^{16}O, a single shift for each branch gives relative wavelengths

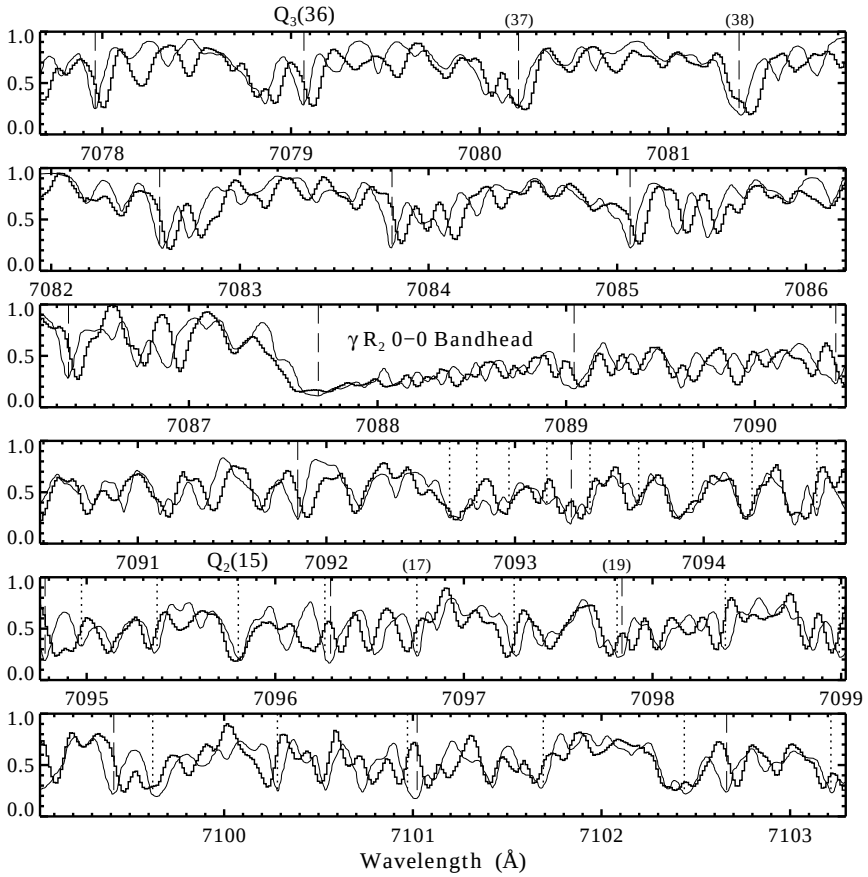

FIG. 1.—One partial echelle order (split into six panels) from an $R = 120{,}000$ observed spectrum of Gl 725B (*histogram*). TiO wavelengths from Jørgensen (1994) were used to generate the synthetic spectrum (*smooth curve*). All the Q_3 0–0 lines (*long-dashed vertical lines*) are 0.05 Å *blueward* of the corresponding feature in the observed spectrum, while the Q_2 0–0 lines (*dotted vertical lines*) are 0.04 Å *redward*, indicating systematic errors in tabulated TiO wavelengths independent of any zero-point errors in the observed wavelength scale. Stellar parameters are from § 3.4.

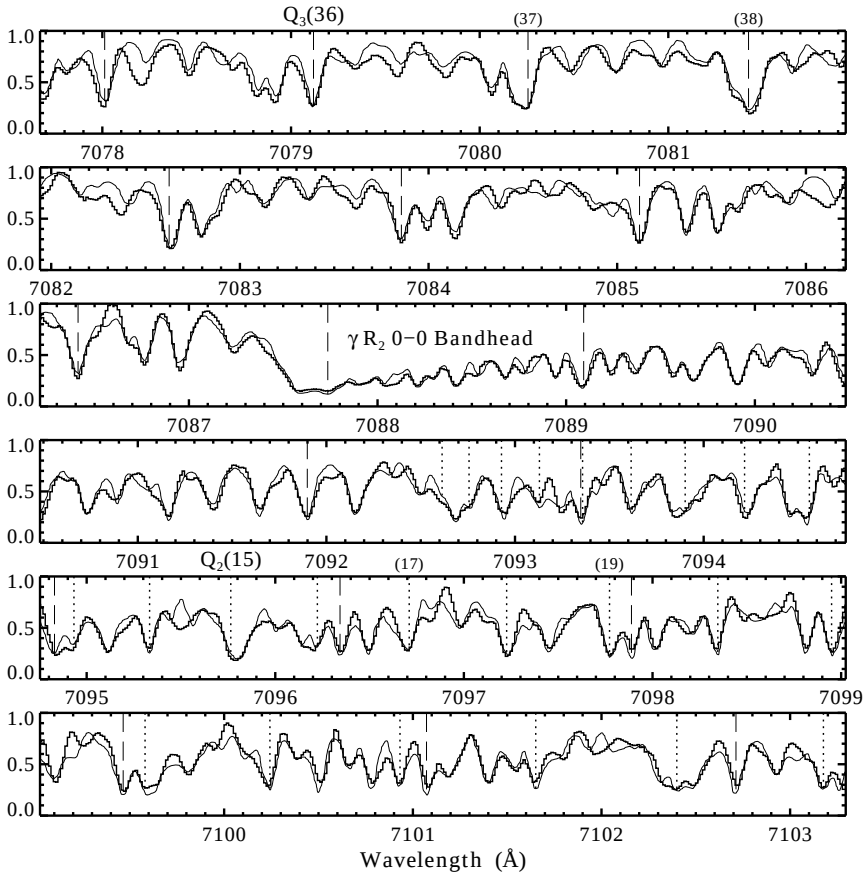

FIG. 2.—Same as Fig. 1, except that wavelengths for the six strongest TiO bands have been empirically corrected, using a total of 10 free parameters. For the strongest band (Q_3), separate shifts were determined for all five isotopes (see Table 2). The fit is greatly improved.

precise to 0.005 Å over our spectral interval with no detectable dependence on rotational quantum number. Shifts for other isotopes (Table 2) are based on only a few weak lines, so results are less certain. Note that the corrections vary systematically with vibrational transition, ΔJ, triplet state, and isotope, suggesting that modified molecular constants might reproduce the observed wavelengths.

To investigate the accuracy and precision of our TiO wavelength corrections, we fit parabolas to the cores of 14 strong atomic lines in our spectrum and compared wavelengths of the line minima with laboratory data. Our measured wavelengths for the atomic lines have rms residuals of 0.005 Å with respect to the laboratory values, which is comparable to the accuracy of our original wavelength solution based on a thorium lamp spectrum (see § 3.1). Averaging the residuals for all 14 lines gives the zero point of the stellar rest frame with an accuracy better than 0.002 Å. After correcting for the barycentric motion (-1.356 ± 0.004 km s^{-1}) of the observatory during the observations, we find that the atomic line cores in our spectrum of Gl 725B are shifted with respect to the laboratory frame by 1.21 ± 0.10 km s^{-1}.

As an aside, we remind the reader that because of gravitational redshifts and surface velocity fields, the apparent

TABLE 1

CORRECTIONS FOR ^{48}Ti^{16}O γ-BANDS

Branch	0–0 (Å)	1–0 (Å)
P_2	−0.040	+0.020
Q_2	−0.035	+0.025
R_2	−0.030	+0.040
P_3	+0.045	+0.095
Q_3	+0.055	+0.105
R_3	+0.070	+0.125

NOTE.—Corrections (in angstroms) must be applied to the line wavelengths described by Jørgensen 1994 in order to match our stellar observations. Corrections have an accuracy of 0.005 Å, and a single shift corrects all lines in a given branch.

TABLE 2

CORRECTIONS FOR γ 0–0 Q_3 BANDS

Isotope	$\Delta\lambda$ (Å)
^{46}Ti^{16}O	+0.120
^{47}Ti^{16}O	+0.090
^{48}Ti^{16}O	+0.055
^{49}Ti^{16}O	+0.030
^{50}Ti^{16}O	−0.025

NOTE.—Corrections (in angstroms) must be applied to the line wavelengths described by Jørgensen 1994 in order to match our stellar observations. Corrections have an accuracy of approximately 0.01 Å.

velocity shift of the line cores differs from the true radial velocity of the star. Photons climbing out of the gravitational potential from any point on the stellar surface suffer a velocity shift of GM_*/cR_*, which is 0.64 km s^{-1} for the Sun. Surface granulation also introduces an apparent shift that depends on spectral type, stellar activity, and line formation depth. For the 14 atomic lines used to establish the velocity zero point, the line cores in the solar spectrum (Kurucz et al. 1984) are systematically redshifted by 0.010 ± 0.002 Å or $+0.43$ km s^{-1}. On the Sun, a net granular blueshift counteracts some of the gravitational redshift, but at this time we can only speculate about how granulation affects the spectrum of Gl 725B.

Figure 2 is identical to Figure 1, except that the synthetic spectrum is based on our empirically corrected TiO wavelengths. Agreement between synthetic and observed spectra is dramatically improved with only 10 free parameters (six from Table 1 and four more from Table 2). Discrepancies still exist, especially in regions of the spectrum where weaker TiO bands dominate, indicating that wavelengths for these bands also need to be corrected. For these weaker bands, however, it is difficult to identify which band corresponds to a particular transition. With better wavelength coverage, one could determine wavelength corrections for strong bands and then iteratively improve the molecular constants. Alternatively, it may be more practical to calculate accurate wavelengths theoretically or to measure them in the laboratory.

Finally, although the wavelength corrections in Table 1 have not been tested outside the wavelength range 7078–7103 Å, they are nonetheless likely to improve tabulated wavelengths for all lines in the relevant bands. This is useful, given that the R_3 0–0 band head near 7055 Å is often used to measure band depth relative to the "continuum" just blueward of the band head.

3.3. *Strength of the ϵ System*

Our interest in TiO was originally motivated by a desire to model weak molecular blends near the magnetic field diagnostic, Fe I 8468.40 Å. Until these TiO blends can be modeled directly, magnetic field measurements for M dwarfs will rely on division by spectra of inactive template stars to remove TiO blends (Johns-Krull & Valenti 1996). Our first attempt to directly model TiO blends near 8468 Å yielded a synthetic spectrum with absorption features deeper than observed (residual intensities of 0.6 instead of 0.8). Moreover, the number, spacing, and relative strengths of the absorption features did not agree with observations. Subsequent analysis revealed that all of the anomalously strong features in the synthetic spectrum were due to the ϵ system ($E\,^3\Pi - X\,^3\Delta$) of TiO, suggesting that the strength of this system may have been overestimated by Jørgensen (1994).

To test this hypothesis, we identified the strongest ϵ band head in our observed spectrum, namely the Q_3 0–0 band head at 8462.53 Å. This also happens to be one of the strongest ϵ band heads at any wavelength (see the Appendix). Figure 3 shows observed and synthetic spectra in the vicinity of this band head. The synthetic spectrum labeled "with ϵ" uses the Simard & Hackett (1991) band oscillator strength (f_{el}) of 0.014 for the ϵ system, as advocated by Jørgensen (1994). The synthetic spectrum labeled "no ϵ" has f_{el} set to zero for the ϵ system. Near the band head, we also show a portion of the spectrum with f_{el} reduced by a factor of 5. All synthetic spectra have been convolved with a Gaussian to match the spectral resolution ($R = 120{,}000$) of the observation.

Using AH atmospheres and model parameters from § 3.4, we generated synthetic spectra of the Q_3 0–0 band head region with f_{el} for the ϵ system reduced by integer factors between 1 and 10. With f_{el} reduced by a factor of 5, the synthetic Q_3 0–0 band head descends to a residual intensity of 0.66, which matches the depth of an unidentified feature observed (but not shown) at 8460.2 Å. There are no deeper features observed in the vicinity, so the strength of the ϵ system must be at least a factor of 5 *below* the Simard & Hackett (1991) value advocated by Jørgensen (1994). If $f_{el} = 0.0028$, then the predicted wavelength of the band head is too red by 2.3 Å. Alternatively, the observed feature at 8460.2 Å is not the ϵ Q_3 0–0 band head, and f_{el} must be even weaker.

Simard & Hackett (1991) measured a lifetime of 770 ± 40 ns for the $E^3\Pi$ ($v = 0$) state of TiO. However, a very similar experiment by Hedgecock, Naulin, & Costes (1995) ruled out lifetimes shorter than 2 μs. Hedgecock et al. (1995) suggest that the analysis by Simard & Hackett (1991) did not properly account for TiO radicals escaping from the detection zone of their apparatus. In any case, the Hedgecock et al. (1995) lower limit on lifetime is a factor of 2.6 higher than the Simard & Hackett (1991) value. After completing our analysis, we became aware of a recent theoretical calculation by Langhoff (1997), who obtains a lifetime of 4.3 μs (with a quoted uncertainty of less than a factor of 2) for the $E\,^3\Pi$ ($v = 0$) state. This is consistent with Hedgecock et al. (1995) and also our own more stringent limit.

Finally, we investigated how reducing the strength of the entire ϵ system affects derived model atmospheres. At our

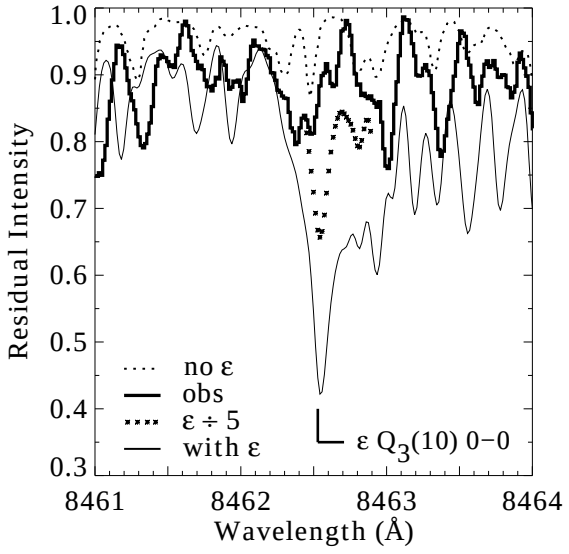

FIG. 3.—Comparison of an observed spectrum (*dark histogram*) of Gl 725B and three synthetic spectra convolved to the same spectral resolution (120,000). Synthetic spectra were computed with the strength of TiO lines in the ϵ system at full (*light curve*), 20% (*asterisks curve*), and zero (*dashed curve*). A deep Q_3 0–0 band head is predicted when using the Simard & Hackett (1991) value of 0.014 for f_{el}, as advocated by Jørgensen (1994). The band head is not obvious in the observation, implying that $f_{el} \leq 0.0028$ for the ϵ system.

request, Peter Hauschildt computed atmospheric models for Gl 725B with f_{el} at the Simard & Hackett (1991) value of 0.014 and also at our new upper limit of 0.0028. When placed on identical continuum optical depth scales, the maximum fractional discrepancy between the two model atmospheres is 0.0073, 0.063, and 0.039 for temperature, electron density, and total particle density, respectively. Discrepancies in the models are largest at $\log \tau_c = -3.5$, -1.2, and $+1.9$, where τ_c is the continuum optical depth at 1.2 μm.

As just described, changes in the strength of the ϵ system do have a global effect on model atmospheres. To quantify how these atmospheric differences affect line depths, we compared synthetic spectra for the portion of echelle order 41 that is in our observed spectrum (8458–8490 Å). Because we want to isolate atmospheric changes in line depth rather than changes due to a modified f_{el}, we suppressed all the ϵ lines in the synthetic spectra but not in the calculation of the atmospheres. The synthetic spectra for both atmospheres ($f_{el} = 0.014$ and 0.0028) were convolved with a Gaussian to match our observed resolution ($R = 120{,}000$). For the atmosphere based on a reduced f_{el}, atomic lines get weaker by as much as 1% of their line depth, while TiO lines (not from the ϵ band) get stronger, again by as much as 1% of their line depth. (Note that these are changes in line depth, not residual intensity.) This error is small compared with other uncertainties, but the high value for f_{el} should nonetheless be avoided, even when computing atmospheres.

3.4. *Stellar Parameters for Gl 725B*

Broadband photometry and spectroscopic analysis provide complementary constraints on stellar parameters. Spectroscopic analyses of M dwarfs are rare, however, because the stars are faint, molecular line data are scarce, and realistic model atmospheres have only recently become available. We present here one of the first detailed spectroscopic analyses of an M dwarf.

Ideally, stellar parameters should be determined using a flux-calibrated observed spectrum, but in fact we have no flux calibration data for our spectrum of Gl 725B. The usual compromise is to normalize the continuum to unity and model the residual intensity. However, cool M dwarfs have such prevalent molecular bands that in general it is not possible to determine the continuum level using only the observed spectrum, even at very high spectral resolution. The only recourse is to normalize observations using model spectra synthesized with and without line opacity, but it is important to realize that this procedure may introduce additional degenerate combinations of model parameters that yield acceptable fits to the observations. For this reason, we strongly advocate the use of flux-calibrated spectra in spectroscopic analysis, even though we have no such calibration for the data presented here.

Molecular features dominate our optical spectrum of Gl 725B, but the spectrum also contains a few prominent atomic lines that can be used to constrain a model. Here we focus on atomic lines in echelle order 40 (8670–8701 Å) because this order has relatively weak stellar molecular features and minimal telluric contamination. Wavelength uncertainties generally make it difficult to identify and model specific molecular features. For strong lines in echelle order 49 (7078–7103 Å), however, we have determined wavelengths accurate to 0.005 Å (see § 3.2). With proper normalization of the observed spectrum, strong TiO features in order 49 can now be used to constrain models. Below, we show that when both molecular and atomic lines are used together as model constraints, stellar parameters can be determined more accurately.

Table 3 gives data for the five atomic lines we used in our analysis of Gl 725B. Initially, we obtained data from VALD (Piskunov et al. 1995) for 35 potentially interesting atomic lines in echelle order 40. We increased the van der Waals damping constants (Γ_6) by a factor of 2.5, based on a previous analysis of the Sun (Valenti & Piskunov 1996). With the solar spectrum (Kurucz et al. 1984) as a constraint, we then used the spectrum-matching program SME (Valenti & Piskunov 1996) to determine empirical log *gf* values for all 35 lines and log Γ_6 for the strong Fe I line at 8688.626 Å. Table 3 gives the empirical log *gf* values from SME, which are larger than the original VALD values by 0.023 to 0.044 (corrections added to log *gf*).

In solving for more precise line data with SME, we adopted most solar model parameters from the $\Delta\Gamma_6 = 2.5$ case given in Table 2 of Valenti & Piskunov (1996). In particular, $\log (\mathrm{Fe/H}) = -4.51$. We did, however, solve for a new macroturbulence (3.04 km s^{-1}) because the macroturbulence formulation in SME is now radial tangential, rather than isotropic Gaussian. For the Fe I 8688.626 Å line, our empirical log Γ_6 after all corrections (-7.701) is half the theoretical FWHM ($2w/N = -7.442$ at 10,000 K) of Anstee et al. (1997). The cause of this discrepancy is unknown. For the γ system of TiO, we simply adopted $f_{el} = 0.15$, as advocated by Jørgensen (1994).

Our goal is to determine stellar parameters for Gl 725B by trying to best match observations with synthetic spectra. The program SME is designed for this purpose, but unfortunately it does not include a full molecular equation of state. Instead, we computed a grid of 63 synthetic spectra using an enhanced, but stand-alone, version of the radiative transfer code used by SME. The regular grid covers $T_{\rm eff} =$ [3000, 3100, 3200, 3300, 3400, 3500, 3600] K, $\log g =$ [4.5, 5.0, 5.5], and [M/H] = [-1.0, -0.5, 0.0]. To generate synthetic spectra for arbitrary values of these three stellar parameters, we used parabolic interpolation in log g and [M/H], followed by cubic spline interpolation in $T_{\rm eff}$. This process was done independently for each wavelength with appropriate checks for excursions outside the grid. Our grid is too coarse to permit accurate interpolation of the residual intensity, but the logarithm of the line depth (one minus the residual intensity) is well behaved. After interpolation in the grid of flux spectra, macroturbulence is added by convolution with a Gaussian.

We fit our observed spectrum of Gl 725B using nonlinear least squares to solve for $T_{\rm eff}$, log g, [M/H], $v_{\rm mac}$, and the continuum normalization factor for echelle order 49. We minimized χ^2 using the Marquardt algorithm (Marquardt

TABLE 3

ATOMIC LINE DATA

$\lambda_{\rm air}$ (Å)	Ion	χ (eV)	log *gf*	log Γ_6	c[a]
8674.746.....	Fe I	2.831	-1.835	-7.456	c_4
8675.372.....	Ti I	1.067	-1.692	-7.438	c_2
8682.980.....	Ti I	1.053	-1.985	-7.438	c_2
8688.626.....	Fe I	2.176	-1.237	-7.701	c_3
8692.331.....	Ti I	1.046	-2.318	-7.438	c_2

[a] Constraint nomenclature used in Table 4.

1963; Press et al. 1986), except that highly discrepant points in echelle order 49 were ignored during the fitting procedure. These discrepancies are dominated by misplaced TiO opacity, due to TiO wavelength errors for bands not corrected in § 3.2. To prevent rejection of good spectrum points due to a poor initial guess for the stellar parameters, we gradually reduced the outer threshold from 0.15 residual intensity units down to 0.04 in steps of 0.01 per iteration. This iterative data selection process ultimately retains approximately half of the 2048 pixels in echelle order 49.

For most calculations described herein, we have set both rotation and microturbulence ($v_{\rm mic}$) to zero. These parameters may actually be nonzero, but in the present analysis, microturbulence, macroturbulence, and rotation all have a similar effect on the spectrum. For example, given the quality of existing line data, we are unable to meaningfully distinguish between $v_{\rm mic} = 1$ km s^{-1} and $v_{\rm mac} = 0.75$ km s^{-1}. In both cases, turbulence simply smooths the spectrum in a very similar manner. By only allowing $v_{\rm mac}$ to be nonzero, we effectively combine the influence of three nearly degenerate parameters into a single quantity with a magnitude of 1.1 ± 0.7 km s^{-1}. We note that microturbulence is 0.75 ± 0.25 km s^{-1} in the Sun (Valenti & Piskunov 1996) and has no obvious dependence on temperature for F, G, and K dwarfs (Gray 1988). One may speculate that moderately cool M dwarfs behave similarly, but this has not yet been demonstrated. Except for the Fe I 8688.626 Å line discussed above, Unsöld values of Γ_6 were enhanced by a factor of 2.5. This is consistent with our analysis of the solar spectrum, but again there is currently no empirical knowledge of whether this enhancement factor is appropriate for M dwarfs. Further study of all of these parameters is needed.

Table 4 gives sets of stellar parameters derived for Gl 725B, using the listed combinations of observational constraints. Note that the three Ti I lines are members of the same multiplet and do not provide independent constraints. The solution based on all available constraints (*last row*) provides the best estimate of actual stellar parameters. Error analysis based on the observed S/N yields formal uncertainties of 1.2 K, 0.0063, 0.0043, and 0.015 km s^{-1} for $T_{\rm eff}$, log g, [M/H], and $v_{\rm mac}$, respectively, but systematic errors are certainly much larger. To better characterize our actual uncertainties, we use the standard deviation of derived parameter values for cases with one constraint removed. For Gl 725B, we obtain $T_{\rm eff} = 3202 \pm 71$ K, log $g = 4.82 \pm 0.14$, [M/H] $= -0.91 \pm 0.07$, and $v_{\rm mac} = 0.8 \pm 0.7$ km s^{-1}. Reduced χ^2 for the final model is 20.8, indicating that our data quality is much better than our knowledge of the relevant molecular data. If we repeat the entire analysis, but consider only atomic lines, we obtain $T_{\rm eff} = 3070 \pm 260$ K, log $g = 4.56 \pm 0.40$, [M/H] $= -0.93 \pm 0.13$, and $v_{\rm mac} = 1.4 \pm 1.2$ km s^{-1}. We conclude that using molecular lines as model constraints can significantly improve the precision of derived stellar parameters.

TABLE 4

GLIESE 725B DERIVED PARAMETERS

$T_{\rm eff}$ (K)	log g[b]	[M/H][c]	$v_{\rm mac}$ (km s^{-1})	Constraints[a]			
				c_1	c_2	c_3	c_4
3462.....	5.10	−0.71	0.0			X	X
2971.....	4.33	−0.89	2.0		X		X
3063.....	4.54	−0.99	2.2		X	X	
3067.....	4.56	−0.93	2.0		X	X	X
3266.....	5.78	−0.66	0.4	X			
3229.....	4.88	−0.84	0.5	X		X	X
3199.....	4.84	−0.92	0.8	X	X		X
3182.....	4.79	−1.00	0.9	X	X	X	
3202.....	4.82	−0.91	0.8	X	X	X	X

[a] Possible fit constraints are as follows: (c_1) TiO γ-bands 7078–7103 Å; (c_2) Ti I 8675.37, 8682.98, 8692.33 Å; (c_3) Fe I 8688.63 Å; (c_4) Fe I 8674.75 Å.

[b] Logarithm of the surface gravity in cm s^{-2}.

[c] Logarithmic offset in abundances relative to solar values for all elements other than hydrogen.

Figures 2 and 4 show our fits to the observed spectrum. Although the strong molecular lines with corrected wavelengths (see § 3.2) are well fitted, it is clear from discrepancies elsewhere in the spectrum that better wavelengths are needed for all TiO lines. Also, our synthetic spectrum is too deep in the cores of the atomic lines, but not in TiO features. Hauschildt et al. (1997) predict this behavior for an LTE analysis such as the one we have used here. Note that one can compensate for the line core discrepancy by increasing $v_{\rm mac}$, but then the TiO lines will be poorly fitted (see Table 4). This again illustrates the value of including TiO as a fit constraint.

Table 5 cites stellar parameters for Gl 725B, either directly from the literature or using general relations applicable to M dwarfs. Extensive table notes review the various ways in which stellar parameters for M dwarfs have been determined in the past. Note that the spectrum synthesis technique employed here is the only technique with adequate constraints to unambiguously determine $T_{\rm eff}$, log g, and [M/H], rather than assuming one or more of these parameters.

Stellar structure codes yield both $T_{\rm eff}$ and gravity as a function of stellar mass, [M/H], and age. This defines an implicit relationship between $T_{\rm eff}$ and gravity for a given [M/H] and age. D'Antona & Mazzitelli (1985, 1994) only

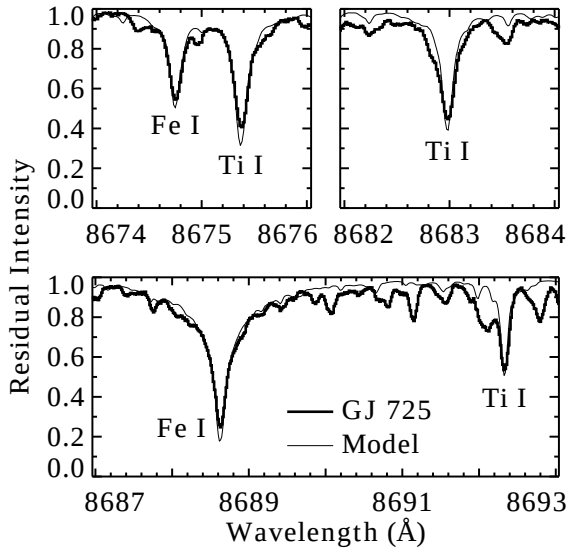

FIG. 4.—Atomic lines observed in echelle order 40 (*dark histogram*), along with the best-fit synthetic spectrum (*light curve*). Except for possible non-LTE effects in the cores of atomic lines, discrepancies are due to errors in the tabulated wavelengths of weak TiO lines. Telluric lines are negligible over most of the order. Only very limited wavelength intervals, where TiO wavelength errors have minimal impact, were considered during the fitting procedure.

TABLE 5

COMPARISON OF GLIESE 725B PARAMETERS

$T_{\rm eff}$ [a]	log g [a]	[M/H] [a]	References	Notes
3300	N/A	...	1	[b]
(3300)	5.00	(0)	2	[c]
(3202)	4.91	N/A	3	[d]
3206	4.89	(0)	4	[e]
3218	N/A	−1.0	5	[f]
(3100)	(5)	(0)	6	[g]
3400	(5)	(0)	7	[h]
3240	4.83	N/A	8	[i]
3620	(5)	(0)	9	[j]
3202	4.82	−0.91	10	

[a] Parentheses indicate assumed rather than derived quantities. N/A indicates that gravity or metallicity was not addressed.

[b] $T_{\rm eff}$ is determined by visual fit of blackbody to observed broadband colors. Line blocking affects short wavelengths, but total flux under the blackbody curve is forced to match the total stellar flux. Metallicity is not specified.

[c] Gravity prediction from stellar structure calculation, assuming solar metallicity. $T_{\rm eff}$ and bolometric magnitude were taken from Veeder 1974.

[d] Fits mass and radius (hence gravity) as a function of $T_{\rm eff}$ for many eclipsing binaries. Data for later M dwarfs are from Popper 1980. Metallicity is an average over stars in the sample. Using our derived $T_{\rm eff}$ yields the gravity in the table.

[e] $T_{\rm eff}$ determined as in Veeder 1974. Radius then follows from measured luminosities. Mass is determined using the mass-luminosity relation of Neece 1984, from which gravity can be calculated.

[f] Comprehensive IR photometry for 322 cool dwarfs. Establishes color-temperature relations based on temperatures for 11 stars from Berriman & Reid 1987 and IR photometry. When tabulated colors for Gl 725B are converted to $T_{\rm eff}$ using these relations, $I-J$ gives $T_{\rm eff} = 3218$ K, while $R-I$ gives $T_{\rm eff} = 3252$ K. Stellar population class is assigned from location in $J-H$ vs. $H-K$ diagram. (Kinematics are used to statistically characterize regions of diagram occupied by each population class.) Gl 725B falls in the old disk/halo region of the color-color diagram, for which Leggett adopts [M/H] ~ -1.0 from Carney, Latham, & Laird 1990 (quote uncertainty of 0.5). For reference, Berriman & Reid 1987 determine $T_{\rm eff}$ using blackbody curves fit to observed 2.2 μm fluxes.

[g] $T_{\rm eff}$ for Gl 725B and EV Lac assumed to be equivalent because of good match in depth of observed TiO features. Temperature of EV Lac (and hence Gl 725B) follows from spectral type of M4.5 Ve and spectral type–temperature relation in Table 1 of Neff et al. 1995, who used colors from Gliese 1969 and the $R-I$ vs. temperature relation of Bessel 1991. Note that direct use of $R-I = 1.15$ for Gl 725B (Gliese 1969) and the Bessel 1991 color-temperature relation gives $T_{\rm eff} = 3205$ K.

[h] Low-resolution ($R \sim 250$), 1.0–2.4 μm spectra of 13 M dwarfs are fit with synthetic spectra based on Allard & Hauschildt 1995a models, deriving an $I_C - K_{\rm CIT}$ vs. temperature relation (see their Fig. 17). [M/H] = 0 curve best matches observations. Using this color-temperature relation and colors from Leggett 1992, we get $T_{\rm eff} = 3400$ K for Gl 725B.

[i] Cubic relation between $T_{\rm eff}$ and $V-K$ color is derived, using photometry and temperature determinations from Berriman & Reid 1987; Leggett 1992; Tinney, Mould, & Reid 1993; and Jones et al. 1996. Combining this relation with $V-K$ from Leggett 1992 gives $T_{\rm eff} = 3240$ K. The relationship between $T_{\rm eff}$, M_K, and log g is derived, using the mass vs. M_K relation of Henry & McCarthy 1993, $M_{\rm bol}$ vs. M_K relation of Tinney et al. 1993 and Jones et al. 1994, and definition of $T_{\rm eff}$. With this relation, $T_{\rm eff}$ from above, and M_K from Henry & McCarthy 1993, infer log $g = 4.83$.

[j] Color-temperature relation from Leggett et al. 1996 is combined with $R-I$ colors from Gliese 1969.

REFERENCES.—(1) Veeder 1974; (2) VandenBerg et al. 1983; (3) Harmanec 1988; (4) Caillault & Patterson 1990; (5) Leggett 1992; (6) Johns-Krull & Valenti 1996; (7) Leggett et al. 1996; (8) Jones et al. 1996; (9) Zboril, Byrne, & Rolleston 1997; (10) This paper.

consider solar metallicity stars, so their results cannot be applied to Gl 725B. For [M/H] of 0.0, −0.5, and −1.5, Baraffe et al. (1995) tabulate $M_{\rm bol}$, $T_{\rm eff}$, and mass. Radius can be computed from the first two quantities and then combined with mass to give log g. Interpolating their results to $T_{\rm eff} = 3202$ K and [M/H] $= -0.91$ yields a mass of 0.12 $M_\odot$ and log $g = 5.23$. This is marginally inconsistent with our measured log $g = 4.83 \pm 0.14$, probably indicating a shortcoming in at least one of the analyses. VandenBerg et al. (1983) do not consider any low-metallicity cases with $T_{\rm eff} < 3500$ K, but a plausible extrapolation also yields a gravity significantly above our spectroscopic value. It seems that stellar structure calculations systematically give higher gravities and/or lower temperatures, relative to the spectroscopic determinations in Table 5.

4. CONCLUSIONS

Discussion of our results appears in preceding sections, immediately following the analysis. Accordingly, we limit our concluding remarks here to a summary of the main points in the paper and a discussion of additional applications for high-resolution molecular spectroscopy.

We have used the best available equation of state, molecular data, and model atmospheres to model the detailed spectrum of an inactive M dwarf. In general, better wavelengths are needed in order to extract the stellar information contained in high-resolution spectra. Some wavelength corrections can be determined empirically (as in § 3.2), but ultimately a new line list will be required, based on either laboratory measurements or theoretical calculations. The electronic oscillator strength for the γ system yields good agreement with observations, but the same is not true of the ϵ system. The problem with the ϵ system has already been noted in recent laboratory and theoretical work and will likely be resolved in the near future.

Spectrum synthesis is a very effective tool for determining stellar parameters from high-resolution spectra. Atomic and molecular features provide complementary constraints that together allow for a more accurate determination of stellar parameters. The detailed analysis of high-resolution spectra yields stellar properties that are *roughly* consistent with the results of low-resolution spectral fits, photometric analyses, stellar structure calculations, and the study of eclipsing binaries. However, all of these procedures are sufficiently complex that it is difficult to reliably compare results using only published information. It would be extremely valuable to analyze a single object in a self-consistent manner, using as many different techniques as possible.

Spectrum synthesis of molecular features is indeed a valuable tool for determining stellar parameters (as in § 3.4), but some other potential applications should also be noted. TiO bands in template stars have been used to estimate empirically the temperature and covering fraction of starspots in RS CVn systems (Neff, O'Neal, & Saar 1995; O'Neal, Saar, & Neff 1996). A complementary analysis using synthetic spectra will provide a framework in which systematic errors can be assessed. Molecular features have exceptional temperature sensitivity and in many RS CVn systems form only in cool spots. Using molecular lines as an additional constraint on Doppler images should lead to more accurate maps and hence greater understanding of magnetic activity. Measured angular diameters of very cool giants and supergiants depend on whether or not the interferometer bandpass contains a strong molecular feature (Quirrenbach et al. 1993). These measurements provide a spatial constraint on the extent of the molecular line formation region, and spectrum synthesis is the key to understanding these data. Finally, molecular lines provide an exceptionally sensitive probe of isotopic abundance ratios (Lambert & Mallia 1972) by virtue of the large effect isotopic substitution has on the molecular moment of inertia.

TABLE 6

INDIVIDUAL TiO LINES AT STRONG BAND HEADS

λ_{air} (Å)	σ (cm^{-1})	RANK	TRANSITION	ISOTOPE	χ (eV)	NUMBER OF LINES	LINE STRENGTH (S)		
							4000 K	3000 K	2000 K
4626.983.....	21606.300	69	$\alpha\ R_2(8)$ 4–1	48	0.193	11	2.90	2.82	2.66
4760.885.....	20998.623	31	$\alpha\ R_2(9)$ 2–0	48	0.069	12	3.22	3.19	3.14
4763.935.....	20985.178	32	$\alpha\ R_3(9)$ 2–0	48	0.081	12	3.18	3.15	3.08
4804.558.....	20807.748	33	$\alpha\ R_2(9)$ 3–1	48	0.194	12	3.21	3.13	2.96
4807.490.....	20795.060	34	$\alpha\ R_3(9)$ 3–1	48	0.207	13	3.17	3.08	2.91
4849.334.....	20615.624	74	$\alpha\ R_2(8)$ 4–2	48	0.317	12	2.91	2.77	2.51
4851.949.....	20604.514	71	$\alpha\ R_3(9)$ 4–2	48	0.331	12	2.92	2.78	2.50
4954.454.....	20178.222	8	$\alpha\ R_2(9)$ 1–0	48	0.069	13	3.56	3.53	3.47
4956.791.....	20168.710	7	$\alpha\ R_3(10)$ 1–0	48	0.083	13	3.56	3.53	3.46
4998.882.....	19998.890	36	$\alpha\ R_2(9)$ 2–1	48	0.194	13	3.15	3.07	2.91
5002.232.....	19985.496	35	$\alpha\ R_3(10)$ 2–1	48	0.208	13	3.16	3.07	2.90
5166.664.....	19349.456	6	$\alpha\ R_2(10)$ 0–0	48	0.070	13	3.66	3.63	3.58
5169.066.....	19340.463	5	$\alpha\ R_3(11)$ 0–0	48	0.084	13	3.67	3.64	3.56
5328.310.....	18762.454	108	$\beta\ R_1(29)$ 1–0	48	0.554	21	2.85	2.62	2.16
5359.408.....	18653.584	92	$\beta\ R_1(28)$ 2–1	48	0.677	22	2.97	2.68	2.11
5391.153.....	18543.747	107	$\beta\ R_1(28)$ 3–2	48	0.802	21	2.96	2.62	1.95
5423.564.....	18432.930	135	$\beta\ R_1(28)$ 4–3	48	0.926	21	2.90	2.51	1.73
5448.132.....	18349.810	15	$\alpha\ R_2(11)$ 0–1	48	0.197	14	3.51	3.42	3.26
5450.789.....	18340.867	19	$\alpha\ R_3(11)$ 0–1	48	0.210	14	3.47	3.39	3.21
5496.605.....	18187.989	43	$\alpha\ R_2(11)$ 1–2	48	0.321	14	3.16	3.02	2.75
5499.455.....	18178.566	47	$\alpha\ R_3(11)$ 1–2	48	0.334	14	3.12	2.98	2.70
5598.390.....	17857.315	127	$\beta\ R_1(36)$ 0–0	50	0.585	24	2.78	2.53	2.04
5598.400.....	17857.283	125	$\beta\ R_1(36)$ 0–0	49	0.585	24	2.78	2.54	2.05
5598.410.....	17857.250	4	$\beta\ R_1(36)$ 0–0	48	0.585	24	3.91	3.66	3.17
5598.421.....	17857.216	98	$\beta\ R_1(36)$ 0–0	47	0.585	24	2.91	2.66	2.17
5598.432.....	17857.181	86	$\beta\ R_1(36)$ 0–0	46	0.585	24	2.95	2.70	2.21
5629.981.....	17757.116	20	$\beta\ R_1(35)$ 1–1	48	0.706	24	3.66	3.37	2.77
5662.221.....	17656.008	38	$\beta\ R_1(34)$ 2–2	48	0.827	24	3.41	3.06	2.37
5695.146.....	17553.937	77	$\beta\ R_1(34)$ 3–3	48	0.951	23	3.15	2.75	1.95
5758.992.....	17359.330	52	$\alpha\ R_2(12)$ 0–2	48	0.323	14	3.02	2.88	2.61
5761.939.....	17350.451	64	$\alpha\ R_3(12)$ 0–2	48	0.335	14	2.99	2.85	2.57
5810.096.....	17206.644	53	$\alpha\ R_2(12)$ 1–3	48	0.446	14	3.06	2.87	2.50
5813.257.....	17197.286	66	$\alpha\ R_3(12)$ 1–3	48	0.458	14	3.03	2.84	2.45
5847.666.....	17096.094	85	$\gamma'\ R_1(9)$ 1–0	48	0.057	13	2.72	2.70	2.65
5873.424.....	17021.121	83	$\gamma'\ R_2(16)$ 1–0	48	0.081	29	2.77	2.73	2.66
5899.678.....	16945.375	51	$\gamma'\ R_3(24)$ 1–0	48	0.116	32	2.93	2.88	2.78
5950.565.....	16800.467	68	$\gamma'\ R_3(24)$ 2–1	48	0.241	32	2.92	2.82	2.62
6149.359.....	16257.353	59	$\gamma'^{S}R_{21}(22)$ 0–0	48	0.084	32	2.90	2.86	2.79
6158.676.....	16232.759	28	$\gamma'\ R_1(10)$ 0–0	48	0.058	14	3.25	3.23	3.18
6186.998.....	16158.450	27	$\gamma'\ R_2(17)$ 0–0	48	0.083	29	3.28	3.24	3.17
6215.558.....	16084.204	17	$\gamma'\ R_3(27)$ 0–0	48	0.127	33	3.46	3.41	3.31
6239.693.....	16021.992	88	$\gamma'\ R_2(17)$ 1–1	48	0.209	30	2.78	2.69	2.51
6268.860.....	15947.446	58	$\gamma'\ R_3(27)$ 1–1	48	0.252	32	2.96	2.86	2.65
6357.332.....	15725.514	57	$\gamma\ R_3(13)$ 3–1	48	0.213	15	2.95	2.86	2.68
6384.175.....	15659.396	63	$\gamma\ R_2(14)$ 3–1	48	0.202	15	2.94	2.85	2.68
6420.615.....	15570.521	56	$\gamma\ R_3(13)$ 4–2	48	0.337	15	3.00	2.86	2.57
6447.901.....	15504.631	67	$\gamma\ R_2(13)$ 4–2	48	0.324	16	2.96	2.83	2.56
6626.460.....	15086.842	78	$\gamma'\ R_3(30)$ 0–1	48	0.263	34	2.85	2.74	2.51
6651.178.....	15030.773	10	$\gamma\ R_3(14)$ 1–0	48	0.089	16	3.51	3.47	3.40
6680.783.....	14964.168	11	$\gamma\ R_2(15)$ 1–0	48	0.079	16	3.50	3.46	3.40
6683.027.....	14959.142	90	$\gamma'\ R_3(30)$ 1–2	48	0.387	33	2.84	2.68	2.36
6714.474.....	14889.082	9	$\gamma\ R_1(17)$ 1–0	48	0.071	18	3.50	3.47	3.41
6717.532.....	14882.305	16	$\gamma\ R_3(14)$ 2–1	48	0.215	15	3.50	3.41	3.23
6747.568.....	14816.057	18	$\gamma\ R_2(15)$ 2–1	48	0.204	16	3.48	3.40	3.23
6784.583.....	14735.226	29	$\gamma\ R_3(14)$ 3–2	48	0.339	15	3.34	3.20	2.91
6815.132.....	14669.175	30	$\gamma\ R_2(15)$ 3–2	48	0.328	15	3.33	3.19	2.91
6852.413.....	14589.367	49	$\gamma\ R_3(14)$ 4–3	48	0.462	15	3.11	2.92	2.53
6883.469.....	14523.544	50	$\gamma\ R_2(15)$ 4–3	48	0.451	16	3.10	2.91	2.53
7054.061.....	14172.316	62	$\gamma\ R_3(16)$ 0–0	50	0.094	17	2.89	2.85	2.77
7054.124.....	14172.190	55	$\gamma\ R_3(16)$ 0–0	49	0.094	17	2.90	2.86	2.78
7054.189.....	14172.059	2	$\gamma\ R_3(16)$ 0–0	48	0.094	17	4.02	3.99	3.91
7054.257.....	14171.923	46	$\gamma\ R_3(16)$ 0–0	47	0.094	17	3.02	2.98	2.90
7054.327.....	14171.782	42	$\gamma\ R_3(16)$ 0–0	46	0.094	17	3.06	3.02	2.94
7087.470.....	14105.512	65	$\gamma\ R_2(17)$ 0–0	50	0.083	17	2.88	2.84	2.77
7087.532.....	14105.387	61	$\gamma\ R_2(17)$ 0–0	49	0.083	17	2.88	2.85	2.78
7087.598.....	14105.256	3	$\gamma\ R_2(17)$ 0–0	48	0.083	17	4.01	3.98	3.91
7087.667.....	14105.120	48	$\gamma\ R_2(17)$ 0–0	47	0.083	17	3.01	2.97	2.90
7087.738.....	14104.979	44	$\gamma\ R_2(17)$ 0–0	46	0.083	17	3.05	3.01	2.94
7124.861.....	14031.486	14	$\gamma\ R_3(16)$ 1–1	48	0.219	16	3.52	3.42	3.24
7125.454.....	14030.318	60	$\gamma\ R_1(19)$ 0–0	50	0.076	19	2.88	2.85	2.79

TABLE 6—*Continued*

λ_{air} (Å)	σ (cm^{-1})	Rank	Transition	Isotope	χ (eV)	Number of Lines	Line Strength (S)		
							4000 K	3000 K	2000 K
7125.518	14030.192	54	$\gamma\ R_1(19)$ 0–0	49	0.076	19	2.89	2.86	2.80
7125.585	14030.061	1	$\gamma\ R_1(19)$ 0–0	48	0.076	19	4.02	3.99	3.92
7125.654	14029.925	45	$\gamma\ R_1(19)$ 0–0	47	0.076	19	3.01	2.98	2.92
7125.726	14029.784	41	$\gamma\ R_1(19)$ 0–0	46	0.076	19	3.05	3.02	2.96
7158.778	13965.009	13	$\gamma\ R_2(17)$ 1–1	48	0.208	17	3.50	3.42	3.24
7197.374	13890.121	12	$\gamma\ R_1(19)$ 1–1	48	0.201	18	3.51	3.43	3.26
7589.219	13172.953	22	$\gamma\ R_3(18)$ 0–1	48	0.224	17	3.41	3.32	3.13
7627.806	13106.314	23	$\gamma\ R_2(19)$ 0–1	48	0.213	18	3.40	3.31	3.13
7665.705	13041.518	26	$\gamma\ R_3(18)$ 1–2	48	0.348	17	3.40	3.25	2.96
7671.657	13031.400	21	$\gamma\ R_1(22)$ 0–1	48	0.209	19	3.42	3.33	3.16
7704.908	12975.163	25	$\gamma\ R_2(19)$ 1–2	48	0.337	17	3.39	3.25	2.96
7743.011	12911.312	40	$\gamma\ R_3(18)$ 2–3	48	0.471	17	3.25	3.05	2.66
7749.499	12900.503	24	$\gamma\ R_1(22)$ 1–2	48	0.333	18	3.41	3.27	2.99
7782.820	12845.272	39	$\gamma\ R_2(19)$ 2–3	48	0.460	17	3.24	3.05	2.66
7821.000	12782.564	73	$\gamma\ R_3(17)$ 3–4	48	0.590	17	3.02	2.77	2.27
7828.142	12770.903	37	$\gamma\ R_1(21)$ 2–3	48	0.453	18	3.25	3.06	2.68
7839.219	12752.857	320	$\varepsilon\ R_3(35)$ 1–0	48	0.161	38	2.18	2.11	1.98
7861.489	12716.731	72	$\gamma\ R_2(19)$ 3–4	48	0.582	18	3.02	2.77	2.28
7899.123	12656.144	359	$\varepsilon\ R_3(35)$ 2–1	48	0.285	36	2.17	2.05	1.81
7907.611	12642.559	70	$\gamma\ R_1(21)$ 3–4	48	0.575	19	3.03	2.78	2.30
8198.659	12193.758	481	$\delta\ R_1(18)$ 1–0	48	0.519	34	2.03	1.82	1.38
8269.758	12088.923	488	$\delta\ R_1(18)$ 2–1	48	0.645	34	2.09	1.81	1.27
8321.874	12013.216	273	$\varepsilon^S R_{21}(38)$ 0–0	48	0.149	47	2.26	2.20	2.07
8341.851	11984.447	665	$\delta\ R_1(18)$ 3–2	48	0.771	34	1.97	1.64	0.99
8344.320	11980.900	138	$\varepsilon\ R_1(15)$ 0–0	48	0.067	26	2.52	2.50	2.44
8361.832	11955.809	307	$\varepsilon^S R_{32}(52)$ 0–0	48	0.247	40	2.24	2.14	1.93
8389.844	11915.891	266	$\varepsilon^R Q_{32}(20)$ 0–0	48	0.091	58	2.25	2.21	2.14
8393.678	11910.449	147	$\varepsilon\ R_2(27)$ 0–0	48	0.113	42	2.52	2.47	2.38
8414.957	11880.331	1018	$\delta\ R_1(18)$ 4–3	48	0.895	34	1.73	1.35	0.60
8440.825	11843.922	101	$\varepsilon\ R_3(41)$ 0–0	48	0.192	38	2.71	2.63	2.47
8462.528	11813.547	104	$\varepsilon\ Q_3(10)$ 0–0	48	0.083	36	2.65	2.62	2.55
8503.001	11757.317	344	$\varepsilon\ R_3(40)$ 1–1	48	0.311	38	2.21	2.07	1.81
8524.524	11727.631	370	$\varepsilon\ Q_3(9)$ 1–1	48	0.207	35	2.11	2.02	1.85
8859.750	11283.895	1007	$\delta\ R_1(21)$ 0–0	49	0.527	36	1.58	1.36	0.91
8859.802	11283.829	143	$\delta\ R_1(21)$ 0–0	48	0.527	36	2.70	2.48	2.04
8859.856	11283.760	850	$\delta\ R_1(21)$ 0–0	47	0.527	36	1.70	1.48	1.04
8859.912	11283.689	812	$\delta\ R_1(21)$ 0–0	46	0.527	36	1.74	1.52	1.08
8936.900	11186.484	382	$\delta\ R_1(21)$ 1–1	48	0.653	36	2.26	1.99	1.44
9200.446	10866.050	619	$\phi\ R_1(12)$ 2–0	48	0.426	14	1.86	1.68	1.32
9244.658	10814.084	343	$\varepsilon\ Q_3(16)$ 0–1	48	0.219	48	2.17	2.07	1.89
9301.725	10747.738	529	$\phi\ R_1(12)$ 3–1	48	0.554	14	1.98	1.75	1.28
9403.685	10631.206	663	$\phi\ R_1(12)$ 4–2	48	0.680	14	1.92	1.64	1.07
9727.892	10276.894	585	$\delta\ R_1(24)$ 0–1	48	0.662	39	1.98	1.71	1.15
9813.348	10187.402	600	$\delta\ R_1(24)$ 1–2	48	0.788	39	2.03	1.70	1.04
9899.965	10098.270	810	$\delta\ R_1(23)$ 2–3	48	0.909	39	1.90	1.52	0.75
10034.500.....	9962.881	248	$\phi\ R_1(13)$ 1–0	48	0.428	14	2.43	2.25	1.89
10147.357.....	9852.076	350	$\phi\ R_1(13)$ 2–1	48	0.555	15	2.29	2.06	1.59
10260.905.....	9743.052	599	$\phi\ R_1(13)$ 3–2	48	0.681	15	1.99	1.70	1.13
11043.884.....	9052.300	111	$\phi\ R_1(14)$ 0–0	48	0.430	15	2.77	2.59	2.22
11044.123.....	9052.104	684	$\phi\ R_1(14)$ 0–0	46	0.430	15	1.80	1.62	1.26
11171.361.....	8949.004	522	$\phi\ R_1(14)$ 1–1	48	0.557	15	1.99	1.76	1.29
12436.660.....	8038.539	315	$\phi\ R_1(15)$ 0–1	48	0.559	16	2.36	2.12	1.65
12583.820.....	7944.533	389	$\phi\ R_1(15)$ 1–2	48	0.685	16	2.26	1.98	1.40
12731.609.....	7852.313	584	$\phi\ R_1(16)$ 2–3	48	0.812	16	2.05	1.71	1.03

We are indebted to Peter Hauschildt for providing unpublished data that allowed us to validate our opacity and equation of state routines. We also thank U. G. Jørgensen for providing the community with TiO line data in machine readable form. We thank Werner Weiss and his VALD team at the Vienna Astronomical Observatory for providing atomic data and access to computer resources.

APPENDIX A

TiO BAND HEADS

For reference, we tabulate information about TiO lines at selected strong band heads. We identified all band heads in Jørgensen's (1994) line data by searching for inflection points in wavenumber (σ) as a function of lower rotational quantum

number (J''). For each band head, we calculated a logarithmic "line strength" for the bluest line in the band. Line strengths (S) were computed using

$$S = \log_{10}(agf\lambda) - \theta\chi\ , \tag{A1}$$

where the quantities in this formula are isotopic abundance fraction (a), statistical weight (g), oscillator strength (f), wavelength (λ), excitation in eV of the lower level (χ), and $\theta = 5040/T$. We considered temperatures (T) of 4000, 3000, and 2000 K. We assumed isotopic abundance fractions of 0.080, 0.073, 0.738, 0.055, and 0.054 for $^{46}Ti^{16}O$, $^{47}Ti^{16}O$, $^{48}Ti^{16}O$, $^{49}Ti^{16}O$, and $^{50}Ti^{16}O$, respectively (Anders & Grevesse 1989). Values of log gf were calculated using the electronic oscillator strengths, $f_{el}(v_{00})$, given by Jørgensen (1994), namely, 0.17, 0.28, 0.14, 0.15, 0.014, 0.048, and 0.052 for the α, β, γ', γ, ϵ, δ, and ϕ systems, respectively. In § 3.3 we showed that the ϵ bands are weaker than what is predicted here.

Table 6 contains data for 124 TiO band heads, ordered by wavelength. The fourth column gives the band identification, along with J'' for the bluest line in the band (located at the band head). The fifth column indicates the relevant isotope of titanium. The first, second, and sixth columns give the air wavelength, vacuum wavenumber, and lower excitation potential of the line at the band head. In § 3.2 we found small wavelength errors in the Jørgensen (1994) lists; the wavelengths in Table 6 presumably have comparable errors. The seventh column gives the total number of lines in a window extending 2 cm^{-1} redward of the band head. All other things being equal, a higher concentration of lines will yield a deeper band head.

The last three columns of Table 6 give the strength of the bluest line in the band, as described above. It is important to note that these line strengths do *not* include any information about what fraction of the Ti will be in TiO at a given temperature. This information depends on pressure and should be computed separately. The line strengths also do not take into consideration the wavelength dependence of the continuous opacity, which will have a small effect on band depth. Nonetheless, the table can be used to compare *relative line opacities* at the tabulated temperatures. Line strengths in the table *will not* correspond to band depths because radiative transfer effects will cause the depth of strong bands to "saturate." However, two bands with similar line strengths and line densities should have similar depths.

Finally, the third column of Table 6 gives a strength rank for each band, based on the line strength at 3000 K given in the ninth column. For this table, we retained the 12 strongest lines in each electronic system (α, β, etc.) and then the 40 strongest lines not yet included the table. Bands in weak systems have large rank because there are many intervening bands from stronger systems that are not in the table.

REFERENCES

Allard, F. 1990, Ph.D. thesis, Univ. Heidelberg
Allard, F., & Hauschildt, P. H. 1995a, in Bottom of the Main Sequence and Beyond, ed. C. G. Tinney (Berlin: Springer), 32 (AH95)
———. 1995b, ApJ, 445, 433
———. 1998, in preparation (AH98)
Allard, F., Hauschildt, P. H., Alexander, D. R., & Starrfield, S. 1997, ARA&A, 35, 137
Allard, F., Hauschildt, P. H., Baraffe, I., & Chabrier, G. 1996, ApJ, 465, L123
Anders, E., & Grevesse, N. 1989, Geochim. Cosmochim. Acta, 53, 197
Anstee, S. D., O'Mara, B. J., & Ross, J. E. 1997, MNRAS, 284, 202
Auman, J. R. 1969, ApJ, 157, 799
Baraffe, I., Chabrier, G., Allard, F., & Hauschildt, P. H. 1995, ApJ, 446, L35
Bennett, P. D. 1983, M.Sc. thesis, Univ. British Columbia
Berriman, G., & Reid, N. 1987, MNRAS, 227, 315
Bessel, M. S. 1991, AJ, 101, 662
Brett, J. M. 1990, A&A, 231, 440
Brett, J. M., & Plez, B. 1993, Proc. Astron. Soc. Australia, 10, 250
Caillault, J. P., & Patterson, J. 1990, AJ, 100, 825
Carney, B. W., Latham, D. W., & Laird, J. B. 1990, AJ, 99, 572
D'Antona, F., & Mazzitelli, I. 1985, ApJ, 296, 502
———. 1994, ApJS, 90, 467
Gliese, W. 1969, Catalogue of Nearby Stars (Karlsruhe: Braun)
Gray, D. F. 1988, Lectures on Spectral-Line Analysis: F, G, and K Stars (Arva: Gray), 3
Harmanec, P. 1988, Bull. Astron. Inst. Czechoslovakia, 39, 329
Hauschildt, P. H., Allard, F., Alexander, D. R., & Baron, E. 1997, ApJ, 488, 428
Hedgecock, I. M., Naulin, C., & Costes, M. 1995, A&A, 304, 667
Henry, T. J., & McCarthy, D. W., Jr. 1993, AJ, 106, 773
Irwin, A. W. 1988, A&AS, 74, 145
John, T. L. 1988, A&A, 193, 189
Johns-Krull, C. M., & Valenti, J. A. 1996, ApJ, 459, L95
Jones, R. A., Longmore, A. J., Allard, F., & Hauschildt, P. H. 1996, MNRAS, 280, 77
Jones, H. R. A., Longmore, A. J., Jameson, R. F., & Mountain, C. M. 1994, MNRAS, 267, 413
Jørgensen, U. G. 1994, A&A, 284, 179
Kirkpatrick, J. D., Henry, T. J., & McCarthy, D. W. 1991, ApJS, 77, 417
Kirkpatrick, J. D., Kelly, D. M., Rieke, G. H., Liebert, J., Allard, F., & Wehrse, R. 1993, ApJ, 402, 643
Kui, R. 1991, Ph.D. thesis, Natl. Univ. Australia
Kurucz, R. L. 1993a, CD-ROM 13 (Cambridge: Smithsonian Astrophys. Obs)
———. 1993b, CD-ROM 18 (Cambridge: Smithsonian Astrophys. Obs)
Kurucz, R. L., Furenlid, I., Brault, J., & Testerman, L. 1984, National Solar Observatory Atlas No. 1 (Tucson: Natl. Sol. Obs.)
Lambert, D. L., & Mallia, E. A. 1972, MNRAS, 156, 337
Langhoff, S. R. 1997, ApJ, 481, 1007
Leggett, S. K. 1992, ApJS, 82, 351
Leggett, S. K., Allard, F., Berriman, G., Dahn, C. C., & Hauschildt, P. H. 1996, ApJS, 104, 117
Marquardt D. W. 1963, J. SIAM, 11, 431
Mould, J. R. 1976, ApJ, 210, 402
———. 1978, ApJ, 226, 923
Naftilan, S. A., Sandmann, W. S., & Pettersen, B. R. 1992, PASP, 104, 1045
Neece, G. D. 1984, ApJ, 277, 738
Neff, J. E., O'Neal, D., & Saar, S. 1995, ApJ, 452, 879
O'Neal, D., Saar, S., & Neff, J. E. 1996, ApJ, 463, 766
Phillips, J. G., & Davis, S. P. 1987, PASP, 99, 839
Piskunov, N. E., Kupka, F., Ryabchikova, T. A., Weiss, W. W., & Jeffery, C. S. 1995, A&AS, 112, 525
Popper, D. M. 1980, ARA&A, 18, 115
Press, W. H., Flannery, B. P., Teukolsky, S. A., & Vetterling, W. T. 1986, Numerical Recipes (Cambridge: Cambridge Univ. Press), 523
Quirrenbach, A., Mozurkewich, D., Armstrong, J. T., Buscher, D. F., & Hummel, C. A. 1993, ApJ, 406, 215
Reid, I. N., Hawley, S. L., & Gizis, J. E. 1995, AJ, 110, 1838
Sauval, A. J., & Tatum, J. B. 1984, ApJS, 56, 193
Schweitzer, A., Hauschildt, P. H., Allard, F., & Basri, G. 1996, MNRAS, 283, 821
Simard, B., & Hackett, P. A. 1991, J. Mol. Spectrosc., 148, 128
Tinney, C. G., Mould, J. R., & Reid, I. N. 1993, AJ, 105, 1045
Tull, R. G., MacQueen, P. J., Sneden, C., & Lambert, D. L. 1995, PASP, 107, 251
Valenti, J. A. 1994, Ph.D. thesis, Univ. California, Berkeley
Valenti, J. A., & Piskunov, N. E. 1996, A&AS, 118, 595
VandenBerg, D. A., Hartwick, F. D. A., Dawson, P., & Alexander, D. R. 1983, ApJ, 266, 747
Veeder, G. J. 1974, AJ, 79, 1056
Zboril, M., Byrne, P. B., & Rolleston, W. R. J. R. 1997, MNRAS, 284, 685